Ultrasensitive Size-Selection of Plasmonic Nanoparticles by Fano Interference Optical Force

Zhipeng Li,[†,*] Shunping Zhang,[‡] Lianming Tong,[§] Peijie Wang,[†] Bin Dong,[⊥] and Hongxing Xu[‡,§,∥]

[†]Beijing Key Laboratory of Nano-Photonics and Nano-Structure (NPNS), Department of Physics, Capital Normal University, Beijing 100048, PR China, [‡]Center for Nanoscience and Nanotechnology and School of Physics and Technology, Wuhan University, Wuhan 430072, PR China, [§]Beijing National Laboratory for Condensed Matter Physics and Institute of Physics, Chinese Academy of Sciences, Box 603-146, Beijing 100190, PR China, [⊥]School of Science, Dalian Nationalities University, Dalian 116600, PR China, and [∥]Division of Solid State Physics/The Nanometer Consortium, Lund University, Box 118, S-22100 Lund, Sweden

ABSTRACT In this paper, we propose a solution for the ultrasensitive optical selection of plasmonic nanoparticles using Fano interference-induced scattering forces. Under a Gaussian beam excitation, the scattering of a plasmonic nanoparticle at its Fano resonance becomes strongly asymmetric in the lateral direction and consequently results in a net transverse scattering force, that is, Fano interference-induced force. The magnitude of this transverse scattering force is comparable with the gradient force in conventional optical manipulation experiments. More interestingly, the Fano scattering force is ultrasensitive to the particle size and excitation frequency due to the phase sensitivity of the interference between adjacent plasmon modes in the particle. Utilizing this distinct feature, we show the possibility of size-selective sorting of silver and gold nanoparticles with an accuracy of about ±10 nm and silica-gold core−shell nanoparticles with shell thickness down to several nanometers. These results would add to the toolbox of optical manipulation and fabrication.

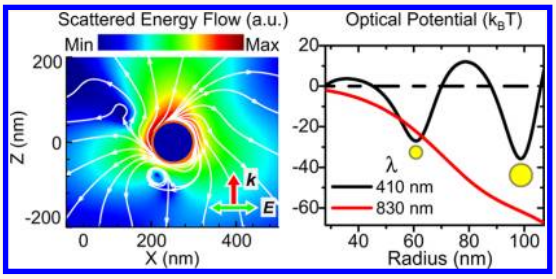

KEYWORDS: size-selective · optical sorting · surface plasmons · Fano resonance · scattering forces

Using light to manipulate objects has been an intense research subject for over 10 years.[1−4] Optical forces due to the light−matter interaction have been well-developed for various optical manipulation techniques to capture particles,[5,6] bacteria,[7] and cells[8] with the size varying from tens of nanometers to several micrometers and exhibited vital applications in physics,[9,10] biology,[11] and chemistry.[12,13] The basic physical mechanism of optical manipulation is the "gradient force" originated from the polarization of small objects by an inhomogeneous light field.[14−16] For plasmonic nanoparticles, the gradient force can be greatly enhanced and changed from attractive to repulsive depending on the red-shifted or blue-shifted laser frequency relative to the dipolar surface plasmon peak of particles.[16] As the surface plasmon can be tuned effectively by the particle size and shape, size-selective trapping and sorting of particles can be realized utilizing the attractive or repulsive nature of the gradient force.[17−20] However, based on this mechanism, the size-selectivity is restricted by the broad width of the dipolar plasmon resonance. On the other hand, Fano resonance originated from the interference between a narrow and broad state and has a narrower line width than a usual dipolar plasmon peak. Fano resonance had been ubiquitously observed in atomic physics[21,22] and classical optics.[23−29] While much attention had been paid to its potential applications in sensing,[30−34] nanoantennas,[35,36] and optoelectronic devices,[37,38] little is known about the optical force on nanoparticles at the Fano resonance and its application on the size-selective optical manipulation.[39]

In this theoretical paper, we propose a single-beam solution for the ultrasensitive optical sorting using the Fano interference-induced scattering force. We found that, in an inhomogeneous light beam, the asymmetric scattering of a plasmonic nanoparticle at its Fano resonance will generate a force that drags the particle to the beam center, which is similar to the function of the conventional gradient force. The magnitude

* Address correspondence to zpli@cnu.edu.cn.

Received for review October 15, 2013 and accepted December 5, 2013.

Published online December 05, 2013
10.1021/nn405364u

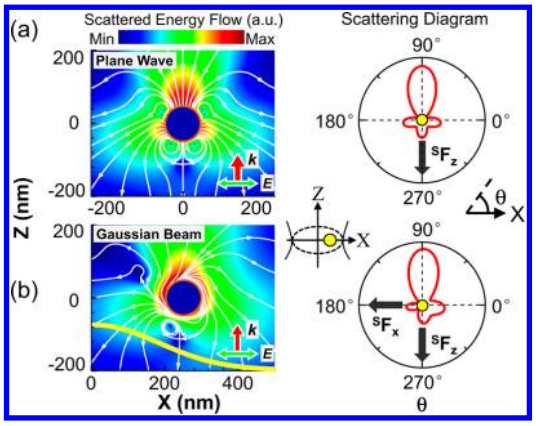

Figure 1. Scattered energy flow $S_{scattering}$ around a silver nanoparticle (R = 50 nm) excited at the wavelength λ = 395 nm. (a) Plane wave excitation. (b) Gaussian beam excitation with the coordinate shown in the inset. $S_{scattering}$ is defined in formula 6 in Methods. The yellow curve in (b) represents the Gaussian profile of the incident intensity. The beam waist w_0 = 0.5 μm. The particle is positioned at $x = w_0/2$. The wave vector and polarization are indicated by red and green arrows. The white line and color scale are the direction and logarithmic modulus of the energy flow, respectively. Right columns in (a) and (b) are the corresponding scattering diagrams in x–z plane. The black arrows indicate the resulting scattering forces along x and z, which are calculated by formula 7 in Methods. The 3D pattern of the scattered energy is shown in Figure S2 in the Supporting Information.

of this attractive scattering force at the Fano resonance frequency is comparable with the gradient force at near-infrared excitation under the same incident power. More importantly, this Fano interference-induced force is ultrasensitive to the particle size, thus it can be utilized for size-selective manipulating and sorting of, for example, silver, gold, and core/shell nanoparticles, with the size-selectivity of only several nanometers. We also reveal that this new force forms a nonconservative field due to the polarization-dependent Fano scattering, obviously different from the conservative gradient force. The ultrasensitive optical selection would work for various nanostructures exhibiting Fano resonance and will certainly open new perspectives in the development of optical nanomanipulation and fabrication.[40,41]

RESULTS AND DISCUSSION

To illustrate the light-scatterer interaction, we first revisit the anomalous scattering of a single plasmonic nanoparticle at Fano resonance, where directional scattering sensitive to the incident frequency of light was observed.[42] As an example, Figure 1 shows the scattered energy flow around a silver particle (R = 50 nm) excited by a plane wave at λ = 395 nm close to the quadrupole resonance of the particle. The white lines and color maps are the direction and logarithmic modulus of the energy flow, respectively. As expected, quadrupolar optical whirlpools and saddles appear around the nanoparticle, and a dominant forward scattering is observed as shown in the far-field scattering diagram in Figure 1a, which is consistent with previous reports.[23,43] The directional scattering will result in a longitudinal interaction $^{S}F_z$ exerted on the particle, which is defined in formula 7 in Methods. Qualitatively, the force $^{S}F_z$ is proportional to the cross section difference between the backward and forward scattering, that is, $W_{BS} - W_{FS}$. If only the first two modes are included,[23] the scattering cross sections can be simply expressed as $W_{BS} \sim |3a_1 - 5a_2|^2$ and $W_{FS} \sim |3a_1 + 5a_2|^2$, where a_n is the Mie scattering coefficient. Hence, the physical meaning of $^{S}F_z$ is a component of the scattering force that contains the coupling term a_1a_2. It represents the contribution from the Fano interference between the dipole and the quadrupole. In the case in Figure 1a, the Fano interference-induced force $^{S}F_z$ is backward force in the longitudinal direction, as shown by the black arrow in the scattering diagram in Figure 1a. When the excitation frequency is off the resonance, a_2 can be neglected, and the scattering is dominated by the normal dipolar mode (see Supporting Information Figure S1). Here we should note, according the definition of formula 7, $^{S}F_z$ could be backward force, while the total longitudinal scattering force calculated by formula 5 is still pushing forward (see Methods).[3] In the transverse direction, on the other hand, the $^{S}F_x$ remains 0 due to the laterally symmetric distribution of the scattering energy. However, a transverse component arises under an inhomogeneous excitation; for example, the particle is positioned off-axis in a Gaussian beam, as shown in Figure 1b. It is obvious that the scattering toward the right significantly surpasses the scattering toward the left in the scattering diagram (for the 3D pattern of the scattered energy, see Figure S2 in the Supporting Information), so that a net transverse scattering force $^{S}F_x$ is induced. More importantly, this transverse scattering force drags the particle to the beam center, similar to the gradient forces in conventional optical manipulation experiments. Notably, these two kinds of forces are essentially different in the sense that the former is a result of Fano interference excited at higher plasmon modes and the latter is originated from the dipolar polarization of particles in an electric field gradient.

To quantify the total optical forces exerted on particles, rigorous electromagnetic calculations of the Maxwell stress tensor are performed (see Methods). Based on the order-of-scattering Mie theory,[44] the time-averaged optical forces contributed by different plasmon modes are analyzed. In expression 3 in the Methods, n represents the scattering field contributed by different plasmon modes. By taking only the n = 1 term (dipolar mode), the dipolar transverse force, that is, the gradient force, $^{1}F_x$ can be obtained by formula 5. As shown by the red circles in Figure 2a, the dipolar

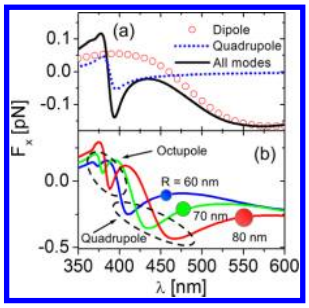

Figure 2. (a) Transverse optical force F_x exerted on a silver nanoparticle as a function of the wavelength of the incident Gaussian beam. The coordinate system is defined in the inset in Figure 1b. The Gaussian beam (w_0 = 0.5 μm and power P = 10 mW) propagates along the z axis with the polarization along the x axis. A silver nanoparticle (R = 50 nm) is positioned at $w_0/2$ on the x axis in the focal plane (z = 0). Individual dipolar and quadrupolar forces are shown by the red circles and dotted blue curves, respectively. Full electromagnetic calculation with the order n up to 12 is shown by the solid curve. (b) Transverse optical forces for silver nanoparticles with radii of 60 nm (blue), 70 nm (green), and 80 nm (red). Dashed circles indicate the transverse scattering forces at the quadrupole and octupole resonances, respectively. The environment is water with the refractive index n_s = 1.33.

transverse force exerted on a silver nanoparticle (R = 50 nm) changes slowly with the wavelength and turns to be repulsive on the blue side of the dipolar resonance at ~460 nm. This tendency is consistent with the behavior of the gradient force predicted by the dipolar approximation, ${}^1F_x \sim \alpha\partial|{}^G\mathbf{E}|^2/\partial x$, where ${}^G\mathbf{E}$ is the electric field of the Gaussian beam and α is the particle polarizability.[45] For the quadrupole mode (only taking n = 2), the transverse force ${}^2F_x$ is relative weak and shifts steeply from attractive to repulsive at the quadrupole resonance λ = 388 nm, as shown by the blue dotted curve. However, as discussed in Figure 1, the optical forces from the coupling term between different modes should be considered when multipoles are excited. An accurate calculation of optical forces must include different modes in the electromagnetic field at the same time. The result is shown by the black solid curve in Figure 2a. Surprisingly, at λ = 395 nm, a prominent asymmetric force dip appears on the slightly red side of the quadrupole resonance, indicating a strong attractive force. Note that with the coordinate system defined in Figure 1b the attractive force is negative and it is the same for the following discussion. Obviously, this profound force dip cannot be comprehended by the simple scalar summation of individual dipolar and quadrupolar forces.

An analytical understanding of the transverse scattering force can be obtained by inserting the electromagnetic expansion into the ${}^S\mathbf{F}$ in formula 7. By using the orthogonality of Legendre functions and neglecting the magnetic amplitude, the transverse scattering force contributed by the interference between different modes can be written as[46]

$$ {}^SF_x \sim \sum_{n=1}^{\infty}\sum_{m=-n}^{n}[K(n,m)a_{nm}a^*_{n-1\,m+1} + J(n,m)a_{nm}a^*_{n+1\,m+1}] \quad (1) $$

where K and J are the polynomials of n and m (see Methods). It is clear that the contributions from the cross terms of neighboring plasmonic modes are nonzero. Obviously, ${}^SF_x$ is the component that contains the interference term and, hence, the origination of the Fano interference force. Here, we take the denotation ${}^{Fano}F_x$. The contribution of ${}^{Fano}F_x$ can be as larger as −0.15 pN at the Fano dip, compared to the weakly repulsive dipolar gradient force at ~0.05 pN. When this force is taken into account, the force dip in Figure 2a can be well-reproduced by $F_x = {}^1F_x + {}^2F_x + {}^{Fano}F_x$. Here, higher modes ($n \geq 3$) are negligible. For example, the octupole force is already about 1 order of magnitude smaller than the former two, even considering its coupling with adjacent modes. Hence, n = 2 is enough for the convergence for the silver particle with R = 50 nm (see Supporting Information Figure S3).

As the particle size increases, the force dip caused by the dipole−quadrupole interference significantly red shifts to 410, 425, and 460 nm for R = 60, 70, and 80 nm, respectively, which is shown in Figure 2b. Furthermore, the octupole becomes non-negligible due to the increasing of the particle size. Hence, high-order Fano dips caused by the interference between adjacent quadrupole and octupole are observed around 370 nm for these particles. Here we noticed that, due to the sharp feature of the dip, at a fixed excitation wavelength, the force will change its sign even for a small variation of the particle size. For example, at λ ~ 410 nm, the transverse force for a particle R = 60 nm is strongly attractive, while for larger particles, R = 70 nm, the force is repulsive.

Utilizing this unique line shape of the Fano interference scattering force, size-sensitive optical selection can be realized. Here we consider the two-dimensional case in the lateral plane (*i.e.*, the focal plane).[47] In Figure 3a, we show the transverse optical potential at the beam center U_0 created by a Gaussian beam of different wavelengths for silver particles with different sizes. The potential U_0 is the work of the optical force moving the particle from infinity to the beam center along the x axis. In our coordinate system, the attractive force will result in a potential well with negative value. At the region of $U_0 < 0$ (the right side of the contour U_0 = 0), there are two steep potential valleys indicated by two white curves, which correspond to the potentials of Fano scattering forces due to the dipole−quadrupole and quadrupole−octupole interference. Notably, the optical potential is ultrasensitive to particle sizes at these valleys. As shown in Figure 3b, at λ = 410 nm (the vertical cross section indicated by the blue line in Figure 3a), the potential well changes its sign sharply as the particle size increases. It is apparent that the

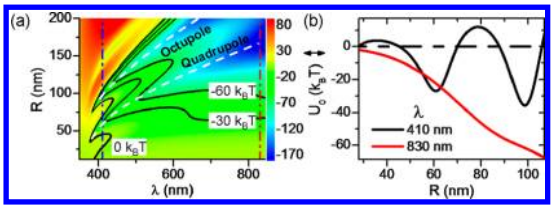

Figure 3. Size-selective optical sorting. (a) Color plot shows optical potential wells at the beam center U_0 as a function of particle radius and excitation wavelength under the incident power of 10 mW. The order n is up to 12. Black curves are contours of $U_0 = 0$, -30, and -60 k_BT, where k_B is the Boltzmann constant and T is the temperature. White dashed curves indicate the optical potential valleys caused by the dipole−quadrupole and quadrupole−octupole Fano interference. (b) Potential well U_0 as a function of the particle radius under the excitation of λ = 410 and 830 nm, corresponding to the cross sections indicated by blue and red vertical lines in (a), respectively. The beam waist for all wavelengths is set to 0.5 μm. The environment is water and T = 300 K.

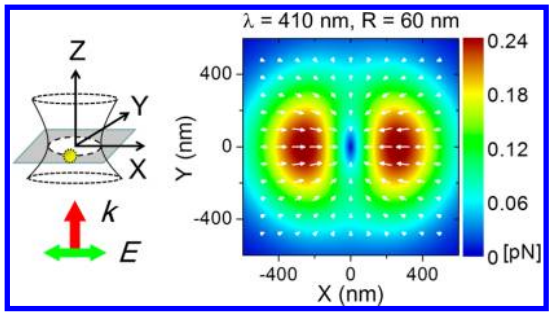

Figure 4. Vector plot of the transverse scattering force for a silver particle (R = 60 nm) at different positions in the focal plane of the Gaussian beam. The excitation is λ = 410 nm with the power of 10 mW. The wave vector and polarization are indicated by red and green arrows in the inset. The white arrows and colors show the direction and magnitude of the optical forces in the focal plane, respectively.

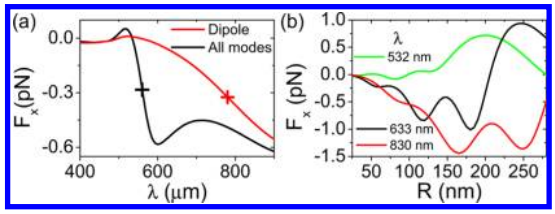

Figure 5. (a) Transverse optical force F_x exerted on a gold nanoparticle (R = 100 nm) as a function of the wavelength of the incident Gaussian beam (power P = 10 mW). The coordinate system is defined in the inset in Figure 1b. The gold nanoparticle is positioned at $w_0/2$ on the x axis in the focal plane (z = 0). Dipolar approximation is shown by the red curve. Full electromagnetic calculation with the order n up to 12 is shown by the black solid curve. The red and black crosses denote the positions of dipole and quadrupole resonances for the gold nanoparticle, respectively. (b) Transverse optical force F_x as a function of the particle radius excited at λ = 532, 633, and 830 nm. The environment is water with n_s = 1.33.

Fano force will only pick particles with $R \sim 60 \pm 11$ nm due to the dipole−quadrupole interference and $R \sim 96 \pm 9$ nm due to the quadrupole−octupole interference. For comparison, as shown by the red curve in Figure 3b, the commonly used near-infrared laser can capture particles with the size widely from tens to hundreds of nanometers without size-selectivity. In practice, such size-selection is important in optical manipulation of metal nanoparticles that exhibit broad size dispersion, such as Ag sol synthesized according to Lee−Meisel's protocol.[48]

For the particles with random Brownian motion in aqueous environment, it is necessary to characterize the scattering force for the particle at different positions in the focal plane of the Gaussian beam (z = 0 plane). In Figure 4, we consider a silver nanoparticle R = 60 nm excited at λ = 410 nm. As discussed above, the dipole−quadrupole interference will result in the attractive scattering force dragging the particle to the beam center (white arrows). Interestingly, the transverse force along the x axis is obviously stronger than the one along the y axis, resulting in a nonconservative force field,[49] which is a consequence of the polarization-dependent Fano interference between adjacent plasmon modes. The ratio of the force in the x and y directions is about 2.7. This is quite different from the case of a gradient force. For example, under the same condition but λ = 830 nm, the transverse gradient force will be conservative (see Supporting Information Figure S4).

The Fano-induced scattering force is expected to exist in other plasmonic materials in which the excitation of Fano resonance is possible. We further study the size-selection of gold nanoparticles in order to expand the generality of this work. Figure 5 shows the transverse optical force F_x exerted on a gold nanoparticle (R = 100 nm) as a function of the wavelength of the incident Gaussian beam. Same as the silver case, the gold nanoparticle is positioned at $w_0/2$ on the x axis in the focal plane. By comparing the dipolar approximation (red curve) and full electromagnetic result (black curve), a prominent force dip appears at the red side of the quadrupole resonance (marked by the black cross). As discussed above, this dip originates from the interference between the dipole and quadrupole excited in the gold nanoparticle, except that it is red-shifted compared to the silver case. Under the incident power of 10 mW, the magnitude of the attractive Fano force can be as large as 0.6 pN at λ = 600 nm, while the gradient force is only 0.03 pN. The size-selection of gold nanoparticles is shown in Figure 5b. Here we consider three commonly used lasers: λ = 532, 633, and 830 nm. At λ = 532 nm, shown by the green curve, the lateral optical force F_x is repulsive for almost all the particles with the size from tens to hundreds of nanometers, while at λ = 633 nm, an attractive force dip appears around R = 110 and 180 nm, corresponding to the Fano scattering force caused by the dipole−quadrupole and quadurpole−octupole interference, respectively. Interestingly, even at λ = 830 nm, the optical force will select particles with a radius around 160 and 250 nm due to the Fano interference.

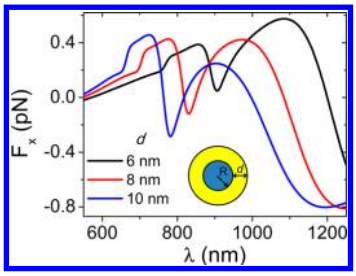

Figure 6. Transverse optical force F_x exerted on a silica–gold core–shell nanoparticle as a function of the wavelength of the incident Gaussian beam (power P = 10 mW). The core radius is R = 100 nm, and the shell thickness is d = 6, 8, 10 nm for the black, red, and blue curves, respectively. The configuration is defined in the inset in Figure 1b. The refractive index of silica is 1.5. The environment is water with n_s = 1.33.

This means that, in conventional experiments of capturing large gold nanoparticles,[50] the trapping mechanism in the lateral plane needs to be reconsidered. In our cases shown here, the main force playing the key role is the scattering force induced by the interference between different plasmon modes rather than the dipolar gradient force. The comparison of the forces contributed by different modes is shown in Figure S5 in Supporting Information.

Furthermore, we show that the Fano interference-induced force can also be extended to metal/dielectric nanoshells. It has been shown that the resonance of surface plasmons of nanoshells can be easily tuned from visible to infrared by varying the shell thickness and the core medium,[51,52] resulting in potential applications in many fields such as imaging and thermal therapy of tumors and cancers.[53,54] Here we consider a representative nanoshell with a silica core (R = 100 nm) and gold shell (thickness d = 6, 8, and 10 nm). Figure 6 shows the transverse force F_x exerted on the silica–gold core–shell particle positioned at $x = w_0/2$ in the focal plane of a Gaussian beam. Similar to the case of solid particles, the interference between the dipolar and quadrupole modes causes prominent force dips appearing at λ = 900, 830, and 785 nm for d = 6, 8, and 10 nm, respectively. This Fano scattering force is ultrasensitive to the shell thickness due to the strong coupling between the outer and inner surface of the shell. For example, at λ = 785 nm, the F_x is attractive for a nanoshell with d = 6 nm and repulsive for the other two cases, while at λ = 830 nm, the optical force will attract only the nanoshell with d = 8 nm. The selectivity of the shell thickness is only a few nanometers.

Finally, we point out that, for the net scattering force in the z direction, it is overwhelmed by the absorption force along the light propagation. The 3D trapping could be possibly realized with the help of the counter-propagating beam setup or the negatively charged substrate, which is a topic of future study. Moreover, from a practical point of view, heating effect is nontrivial in optical manipulation experiments. Optical heating of metallic nanoparticles has been investigated,[55] and the temperature elevation above the boiling point of water has been reported.[56,57] In our cases, the Fano interference force occurs on the red side of the multipole resonance, which already avoids a large portion of light absorption by the particle. On the other hand, considering the much weaker power density used in the present study (~10 mW/μm^2) and the cooling effect due to possible convection, the optical heating is expected not to disturb the optical selection process in the aqueous environment.

CONCLUSIONS

In conclusion, we have investigated the optical force on a plasmonic nanoparticle at its Fano resonance in a Gaussian beam. We found that, under the inhomogeneous excitation, the lateral asymmetric scattering caused by the Fano interference between adjacent plasmon modes results in a transverse scattering force. The Fano interference-induced scattering force could attract or repulse particles into or out of the beam center sensitively depending on the particle size and excitation frequency. Using this distinct feature, the size-selective optical sorting for silver, gold, and core–shell nanoparticles has been proposed. The selection precision can be as narrow as a few nanometers. Although we only focused on spherical particles, the scheme is general for various plasmonic nanostructures exhibiting Fano characteristics.[23,58] Moreover, these findings can also be applied to other optical manipulating techniques, such as surface plasmon tweezers,[59] multiparticle trapping,[60] and optical torque rotations,[61] which will greatly extend the application of optical forces on nanomanipulation, fabrication, and even lab-on-a chip devices, *etc*.

METHODS

Computational Method. The electric field of the incident beam ${}^{i}\mathbf{E}$ is expanded into powers of electrical and magnetic vector spherical harmonics ($\mathbf{M}_{nm}$ and $\mathbf{N}_{nm}$) by introducing the corresponding off-axis Gaussian expansion coefficients ${}^{G}C_{nm1}$ and ${}^{G}C_{nm2}$[62]

$$ {}^{i}\mathbf{E} = \sum_{n=1}^{\infty}\sum_{m=-n}^{n}({}^{G}C_{nm1}\mathbf{M}_{nm} + {}^{G}C_{nm2}\mathbf{N}_{nm}) \qquad (2) $$

where $n \in [1,\infty]$ and $m \in [-n,n]$ are the multipole order and the angular number, respectively. The scattering field can be expressed as

$$ {}^{s}\mathbf{E} = \sum_{n=1}^{\infty}\sum_{m=-n}^{n}(b_{nm}\mathbf{M}_{nm} + a_{nm}\mathbf{N}_{nm}) \qquad (3) $$

where a_{nm} and b_{nm} are the expansion coefficients of Mie scattering. The permittivities of silver and gold were adapted from the experimental data by Johnson and Christy.[63]

The spherical Bessel functions in the vector spherical harmonics take the form of Hankel functions. The magnetic field can be obtained through the relation

$$\mathbf{H} = \frac{1}{i\omega\mu}\nabla \times \mathbf{E} \tag{4}$$

The time-averaged optical force can be computed by the integration of the Maxwell stress tensor $\mathbf{T} = \varepsilon\mathbf{EE} + \mu\mathbf{HH} - 1/2(\varepsilon E^2 + \mu H^2)\delta$ over the surface S enclosing the particle

$$\langle \mathbf{F} \rangle = \oint_S \langle \mathbf{T}\cdot\hat{\mathbf{r}} \rangle dS \tag{5}$$

where the electromagnetic field includes the incident and scattered field $\mathbf{E} = {}^{i}\mathbf{E} + {}^{s}\mathbf{E}$, $\mathbf{H} = {}^{i}\mathbf{H} + {}^{s}\mathbf{H}$; $\hat{\mathbf{r}}$ is the normal unit vector pointing out from the surface, and δ is a unit matrix.

Scattering Energy Flow. The scattering energy flow is calculated by

$$\mathbf{S}_{\text{scattering}} = \frac{1}{2}\,\text{Re}({}^{s}\mathbf{E} \times {}^{s}\mathbf{H}^{*}) \tag{6}$$

The scattering diagram $\mathbf{S}_{\text{scattering}}$ is calculated for $r \gg \lambda$ at different polar angle θ. The force ${}^{s}\mathbf{F}$ showed in the diagram in Figure 1 corresponds to the component

$$\langle {}^{s}\mathbf{F} \rangle = \oint_S \langle \mathbf{T}_s\cdot\hat{\mathbf{r}} \rangle dS \tag{7}$$

where $\mathbf{T}_s = \varepsilon^{s}\mathbf{E}^{s}\mathbf{E} + \mu^{s}\mathbf{H}^{s}\mathbf{H} - 1/2(\varepsilon^{s}E^2 + \mu^{s}H^2)\delta$. $\langle {}^{s}\mathbf{F} \rangle$ is the component containing the coupling term between different modes, which could be the pulling force in the longitudinal direction. The total scattering force computed by formula 5 is still the pushing force as reported in previous work.[3] In an inhomogeneous excitation, $\langle {}^{s}\mathbf{F} \rangle$ will have a transverse component which is the origination of the attractive Fano interference force that can be used for the ultrasensitive size-selection.

Analytical Derivation of ${}^{Fano}F_x$. We focused on the interference term ${}^{s}F_x$ in formula 7. In spherical coordinate system, formula 7 can be written as

$$\langle {}^{s}\mathbf{F} \rangle = \oint_S \left\langle \varepsilon^{s}E_r\,{}^{s}\mathbf{E} + \mu^{s}H_r\,{}^{s}\mathbf{H} - \frac{1}{2}(\varepsilon^{s}E^2 + \mu^{s}H^2)\hat{\mathbf{r}} \right\rangle dS \tag{8}$$

Considering a particle on x axis, the x component ${}^{s}F_x$ can be obtained according to the basis vector transformation:

$${}^{s}F_x = \int_0^{2\pi}\int_0^{\pi} {}^{s}T_r R^2 \sin^2\theta\cos\varphi\, d\theta d\varphi \tag{9}$$

where R is the radius of the integrating sphere, ${}^{s}T_r$ takes the expression

$${}^{s}T_r = \frac{1}{2}[\varepsilon({}^{s}E_r{}^{s}E_r^{*} - {}^{s}E_\theta{}^{s}E_\theta^{*} - {}^{s}E_\varphi{}^{s}E_\varphi^{*}) + \mu({}^{s}H_r{}^{s}H_r^{*} - {}^{s}H_\theta{}^{s}H_\theta^{*} - {}^{s}H_\varphi{}^{s}H_\varphi^{*})] \tag{10}$$

${}^{s}F_x$ can be obtained by inserting 3 and 4 into 9 and using the orthogonality of associated Legendre functions $P_n^m(\cos\theta)$:

$$\begin{aligned}
&\int_0^{2\pi} e^{i(m-m')\phi} d\phi \int_0^{\pi} \left[\frac{dP_n^m(\cos\theta)}{d\theta}\frac{dP_{n'}^{m'}(\cos\theta)}{d\theta} \right. \\
&\left. + mm'\frac{P_n^m(\cos\theta)}{\sin\theta}\frac{P_{n'}^{m'}(\cos\theta)}{\sin\theta} \right] \sin^2\theta e^{i\phi} d\theta \\
&= 4\pi\sqrt{\frac{(n+m)!}{(2n+1)(n-m)!}}\sqrt{\frac{(n'+m')!}{(2n'+1)(n'-m')!}} \\
&\times \left[\sqrt{\frac{(n+m+1)(n+m+2)}{(2n+1)(2n+3)}}\, n(n+2)\delta_{n+1,n'} \right. \\
&\left. - \sqrt{\frac{(n-m-1)(n-m)}{(2n-1)(2n+1)}}\,(n-1)(n+1)\delta_{n-1,n'} \right] \delta_{m+1,m'}
\end{aligned} \tag{11}$$

where $\delta_{m,n}$ is the Kronecker delta. Here, only the terms from adjacent plasmon modes $n' = n-1$, $n+1$ are nonzero. Obviously, ${}^{s}F_x$ is the component that contains the interference term and, hence, the origination of the Fano interference force ${}^{Fano}F_x$. By neglecting the magnetic amplitude, ${}^{Fano}F_x$ is proportional to

$$\begin{aligned}
{}^{s}F_x = {}^{Fano}F_x \sim \sum_{n=1}^{\infty}\sum_{m=-n}^{n} &[K(n,m)a_{nm}a_{n-1\,m+1}^{*} \\
&+ J(n,m)a_{nm}a_{n+1\,m+1}^{*}]
\end{aligned} \tag{12}$$

where

$$\begin{aligned}
K(n,m) &= 4\pi\frac{(n^2-1)(n+m)!}{(4n^2-1)(n-m-2)!}, \\
J(n,m) &= 4\pi\frac{n(n+2)(n+m+2)!}{(2n+1)(2n+3)(n-m)!}
\end{aligned} \tag{13}$$

Conflict of Interest: The authors declare no competing financial interest.

Acknowledgment. Z.P.L. thanks Dr. Bo Wang for the validation test by numerical simulation. This work was supported by the National Natural Science Foundation of China (Grant Nos. 11274004, 11374355, 11227407), NCET (Grant No. NCET-13-0915), Beijing Nova Program (2011079), Beijing Natural Science Foundation (Grant No. 1122012), and MOST (2012YQ12006005).

Supporting Information Available: The scattered energy flow around a dipole, 3D pattern of the scattering energy, convergence of the transverse optical force, the force field of the dipolar gradient force, and comparison of forces on Au nanoparticles including different plasmon modes. This material is available free of charge *via* the Internet at http://pubs.acs.org.

REFERENCES AND NOTES

1. Grier, D. G. A Revolution in Optical Manipulation. *Nature* **2003**, *424*, 810–816.
2. Hansen, P. M.; Bhatia, V. K.; Harrit, N.; Oddershede, L. Expanding the Optical Trapping Range of Gold Nanoparticles. *Nano Lett.* **2005**, *5*, 1937–1942.
3. Chen, J.; Ng, J.; Lin, Z. F.; Chan, C. T. Optical Pulling Force. *Nat. Photonics* **2011**, *5*, 531–534.
4. Yan, Z.; Sweet, J.; Jureller, J. E.; Guffey, M. J.; Pelton, M.; Scherer, N. F. Controlling the Position and Orientation of Single Silver Nanowires on a Surface Using Structured Optical Fields. *ACS Nano* **2012**, *6*, 8144–8155.
5. Guffey, M. J.; Scherer, N. F. All-Optical Patterning of Au Nanoparticles on Surfaces Using Optical Traps. *Nano Lett.* **2010**, *10*, 4302–4308.
6. Lehmuskero, A.; Ogier, R.; Gschneidtner, T.; Johansson, P.; Käll, M. Ultrafast Spinning of Gold Nanoparticles in Water Using Circularly Polarized Light. *Nano Lett.* **2013**, *13*, 3129–3134.
7. Righini, M.; Ghenuche, P.; Cherukulappurath, S.; Myroshnychenko, V.; García de Abajo, F. J.; Quidant, R. Nano-Optical Trapping of Rayleigh Particles and Escherichia Coli Bacteria with Resonant Optical Antennas. *Nano Lett.* **2009**, *9*, 3387–3391.
8. Zhang, H.; Liu, K. K. Optical Tweezers for Single Cells. *J. R. Soc. Interface* **2008**, *5*, 671–690.
9. Juan, M. L.; Righini, M.; Quidant, R. Plasmon Nano-Optical Tweezers. *Nat. Photonics* **2011**, *5*, 349–356.
10. Reece, P. J.; Toe, W. J.; Wang, F.; Paiman, S.; Gao, Q.; Tan, H. H.; Jagadish, C. Characterization of Semiconductor Nanowires Using Optical Tweezers. *Nano Lett.* **2011**, *11*, 2375–2381.
11. Hegge, S.; Uhrig, K.; Streichfuss, M.; Kynast-Wolf, G.; Matuschewski, K.; Spatz, J. P.; Frischknecht, F. Direct Manipulation of Malaria Parasites with Optical Tweezers Reveals Distinct Functions of Plasmodium Surface Proteins. *ACS Nano* **2012**, *6*, 4648–4662.
12. Paik, D. H.; Seol, Y.; Halsey, W. A.; Perkins, T. T. Integrating a High-Force Optical Trap with Gold Nanoposts and a Robust Gold–DNA Bond. *Nano Lett.* **2009**, *9*, 2978–2983.
13. Hormeno, S.; Bastus, N. G.; Pietsch, A.; Weller, H.; Arias-González, J. R.; Juarez, B. H. Plasmon–Exciton Interactions

on Single Thermoresponsive Platforms Demonstrated by Optical Tweezers. *Nano Lett.* **2011**, *11*, 4742–4747.
14. Ashkin, A.; Dziedzic, J. M.; Bjorkholm, J. E.; Chu, S. Observation of a Single-Beam Gradient Force Optical Trap for Dielectric Particles. *Opt. Lett.* **1986**, *11*, 288–290.
15. Ashkin, A. Optical Trapping and Manipulation of Neutral Particles Using Lasers. *Proc. Natl. Acad. Sci. U.S.A.* **1997**, *94*, 4853–4860.
16. Arias-González, J. R.; Nieto-Vesperinas, M. Optical Forces on Small Particles: Attractive and Repulsive Nature and Plasmon-Resonance Conditions. *J. Opt. Soc. Am. A* **2003**, *20*, 1201–1209.
17. Zelenina, A. S.; Quidant, R.; Badenes, G.; Nieto-Vesperinas, M. Tunable Optical Sorting and Manipulation of Nanoparticles *via* Plasmon Excitation. *Opt. Lett.* **2006**, *31*, 2054–2056.
18. Gaugiran, S.; Getin, S.; Fedeli, J. M.; Derouard, J. Polarization and Particle Size Dependence of Radiative Forces on Small Metallic Particles in Evanescent Optical Fields. Evidences for Either Repulsive or Attractive Gradient Forces. *Opt. Express* **2007**, *15*, 8146–8156.
19. Dienerowitz, M.; Mazilu, M.; Reece, P. J.; Krauss, T. F.; Dholakia, K. Optical Vortex Trap for Resonant Confinement of Metal Nanoparticles. *Opt. Express* **2008**, *16*, 4991–4999.
20. Ploschner, M.; Čižmár, T.; Mazilu, M.; Di Falco, A.; Dholakia, K. Bidirectional Optical Sorting of Gold Nanoparticles. *Nano Lett.* **2012**, *12*, 1923–1927.
21. Fano, U. Effects of Configuration Interaction on Intensities and Phase Shifts. *Phys. Rev.* **1961**, *124*, 1866–1878.
22. Miroshnichenko, A. E.; Flach, S.; Kivshar, Y. S. Fano Resonances in Nanoscale Structures. *Rev. Mod. Phys.* **2010**, *82*, 2257–2298.
23. Luk'yanchuk, B.; Zheludev, N. I.; Maier, S. A.; Halas, N. J.; Nordlander, P.; Giessen, H.; Chong, C. T. The Fano Resonance in Plasmonic Nanostructures and Metamaterials. *Nat. Mater.* **2010**, *9*, 707–715.
24. Chuntonov, L.; Haran, G. Trimeric Plasmonic Molecules: The Role of Symmetry. *Nano Lett.* **2011**, *11*, 2440–2445.
25. Zhang, S. P.; Bao, K.; Halas, N. J.; Xu, H. X.; Nordlander, P. Substrate-Induced Fano Resonances of a Plasmonic Nanocube: A Route to Increased-Sensitivity Localized Surface Plasmon Resonance Sensors Revealed. *Nano Lett.* **2011**, *11*, 1657–1663.
26. Svedendahl, M.; Käll, M. Fano Interference between Localized Plasmons and Interface Reflections. *ACS Nano* **2012**, *6*, 7533–7539.
27. Francescato, Y.; Giannini, V.; Maier, S. A. Plasmonic Systems Unveiled by Fano Resonances. *ACS Nano* **2012**, *6*, 1830–1838.
28. Lovera, A.; Gallinet, B.; Nordlander, P.; Martin, O. J. F. Mechanisms of Fano Resonances in Coupled Plasmonic Systems. *ACS Nano* **2013**, *7*, 4527–4536.
29. Zhang, S. P.; Chen, L.; Huang, Y.; Xu, H. X. Reduced Linewidth Multipolar Plasmon Resonances in Metal Nanorods and Related Applications. *Nanoscale* **2013**, *5*, 6985–6991.
30. Hao, F.; Nordlander, P.; Sonnefraud, Y.; Van Dorpe, P.; Maier, S. A. Tunability of Subradiant Dipolar and Fano-Type Plasmon Resonances in Metallic Ring/Disk Cavities: Implications for Nanoscale Optical Sensing. *ACS Nano* **2009**, *3*, 643–652.
31. Liu, N.; Weiss, T.; Mesch, M.; Langguth, L.; Eigenthaler, U.; Hirscher, M.; Soennichsen, C.; Giessen, H. Planar Metamaterial Analogue of Electromagnetically Induced Transparency for Plasmonic Sensing. *Nano Lett.* **2010**, *10*, 1103–1107.
32. Offermans, P.; Schaafsma, M. C.; Rodriguez, S. R. K.; Zhang, Y. C.; Crego-Calama, M.; Brongersma, S. H.; Rivas, J. G. Universal Scaling of the Figure of Merit of Plasmonic Sensors. *ACS Nano* **2011**, *5*, 5151–5157.
33. Pasquale, A. J.; Reinhard, B. M.; Dal Negro, L. Engineering Photonic–Plasmonic Coupling in Metal Nanoparticle Necklaces. *ACS Nano* **2011**, *5*, 6578–6585.
34. Ye, J.; Wen, F. F.; Sobhani, H.; Lassiter, J. B.; Van Dorpe, P.; Nordlander, P.; Halas, N. J. Plasmonic Nanoclusters: Near Field Properties of the Fano Resonance Interrogated with Sers. *Nano Lett.* **2012**, *12*, 1660–1667.
35. Li, Z. P.; Shegai, T.; Haran, G.; Xu, H. X. Multiple-Particle Nanoantennas for Enormous Enhancement and Polarization Control of Light Emission. *ACS Nano* **2009**, *3*, 637–642.
36. Alonso-Gonzalez, P.; Schnell, M.; Sarriugarte, P.; Sobhani, H.; Wu, C.; Arju, N.; Khanikaev, A.; Golmar, F.; Albella, P.; Arzubiaga, L.; *et al.* Real-Space Mapping of Fano Interference in Plasmonic Metamolecules. *Nano Lett.* **2011**, *11*, 3922–3926.
37. Shegai, T.; Chen, S.; Miljković, V. D.; Zengin, G.; Johansson, P.; Käll, M. A Bimetallic Nanoantenna for Directional Colour Routing. *Nat. Commun.* **2011**, *2*, 481.
38. Chang, W. S.; Lassiter, J. B.; Swanglap, P.; Sobhani, H.; Khatua, S.; Nordlander, P.; Halas, N. J.; Link, S. A Plasmonic Fano Switch. *Nano Lett.* **2012**, *12*, 4977–4982.
39. Ridolfo, A.; Saija, R.; Savasta, S.; Jones, P. H.; Iati, M. A.; Marago, O. M. Fano-Doppler Laser Cooling of Hybrid Nanostructures. *ACS Nano* **2011**, *5*, 7354–7361.
40. Novitsky, A.; Qiu, C. W.; Lavrinenko, A. Material-Independent and Size-Independent Tractor Beams for Dipole Objects. *Phys. Rev. Lett.* **2012**, *109*, 023902.
41. Vossen, D. L. J.; Fific, D.; Penninkhof, J.; van Dillen, T.; Polman, A.; van Blaaderen, A. Combined Optical Tweezers/Ion Beam Technique To Tune Colloidal Masks for Nanolithography. *Nano Lett.* **2005**, *5*, 1175–1179.
42. Tribelsky, M. I.; Flach, S.; Miroshnichenko, A. E.; Gorbach, A. V.; Kivshar, Y. S. Light Scattering by a Finite Obstacle and Fano Resonances. *Phys. Rev. Lett.* **2008**, *100*, 043903.
43. Tribelsky, M. I.; Luk'yanchuk, B. S. Anomalous Light Scattering by Small Particles. *Phys. Rev. Lett.* **2006**, *97*, 263902.
44. Li, Z. P.; Xu, H. X. Electromagnetic Energy Flow near Metal Nanoparticles—II: Algorithms for the Calculation of the Light Scattering of Multi-spheres and Photon Energy Transport *via* Linear Chains of Ag Nanoparticles. *J. Quant. Spectrosc. Radiat. Transfer* **2007**, *103*, 394–401.
45. Chaumet, P. C.; Nieto-Vesperinas, M. Time-Averaged Total Force on a Dipolar Sphere in an Electromagnetic Field. *Opt. Lett.* **2000**, *25*, 1065–1067.
46. Li, Z.; Wu, Z.; Shang, Q. Calculation of Radiation Forces Exerted on a Uniaxial Anisotropic Sphere by an Off-Axis Incident Gaussian Beam. *Opt. Express* **2011**, *19*, 16044–16057.
47. Svedberg, F.; Li, Z. P.; Xu, H. X.; Käll, M. Creating Hot Nanoparticle Pairs for Surface-Enhanced Raman Spectroscopy through Optical Manipulation. *Nano Lett.* **2006**, *6*, 2639–2641.
48. Lee, P. C.; Meisel, D. Adsorption and Surface-Enhanced Raman of Dyes on Silver and Gold Sols. *J. Phys. Chem.* **1982**, *86*, 3391–3395.
49. Wu, P. Y.; Huang, R. X.; Tischer, C.; Jonas, A.; Florin, E. L. Direct Measurement of the Nonconservative Force Field Generated by Optical Tweezers. *Phys. Rev. Lett.* **2009**, *103*, 108101.
50. Saija, R.; Denti, P.; Borghese, F.; Maragò, O. M.; Iatì, M. A. Optical Trapping Calculations for Metal Nanoparticles. Comparison with Experimental Data for Au and Ag Spheres. *Opt. Express* **2009**, *17*, 10231–10241.
51. Prodan, E.; Radloff, C.; Halas, N. J.; Nordlander, P. A Hybridization Model for the Plasmon Response of Complex Nanostructures. *Science* **2003**, *302*, 419–422.
52. Bardhan, R.; Grady, N. K.; Ali, T.; Halas, N. J. Metallic Nanoshells with Semiconductor Cores: Optical Characteristics Modified by Core Medium Properties. *ACS Nano* **2010**, *4*, 6169–6179.
53. Hirsch, L. R.; Stafford, R. J.; Bankson, J. A.; Sershen, S. R.; Rivera, B.; Price, R. E.; Hazle, J. D.; Halas, N. J.; West, J. L. Nanoshell-Mediated Near-Infrared Thermal Therapy of Tumors under Magnetic Resonance Guidance. *Proc. Natl. Acad. Sci. U.S.A.* **2003**, *100*, 13549–13554.
54. Lal, S.; Clare, S. E.; Halas, N. J. Nanoshell-Enabled Photothermal Cancer Therapy: Impending Clinical Impact. *Acc. Chem. Res.* **2008**, *41*, 1842–1851.
55. Tribelsky, M. I.; Miroshnichenko, A. E.; Kivshar, Y. S.; Luk'yanchuk, B. S.; Khokhlov, A. R. Laser Pulse Heating of Spherical Metal Particles. *Phys. Rev. X* **2011**, *1*, 021024.

56. Bendix, P. M.; Nader, S.; Reihani, S.; Oddershede, L. B. Direct Measurements of Heating by Electromagnetically Trapped Gold Nanoparticles on Supported Lipid Bilayers. *ACS Nano* **2010**, *4*, 2256–2262.
57. Fang, Z. Y.; Zhen, Y. R.; Neumann, O.; Polman, A.; de Abajo, F. J. G.; Nordlander, P.; Halas, N. J. Evolution of Light-Induced Vapor Generation at a Liquid-Immersed Metallic Nanoparticle. *Nano Lett.* **2013**, *13*, 1736–1742.
58. Woo, K. C.; Shao, L.; Chen, H. J.; Liang, Y.; Wang, J. F.; Lin, H. Q. Universal Scaling and Fano Resonance in the Plasmon Coupling between Gold Nanorods. *ACS Nano* **2011**, *5*, 5976–5986.
59. Righini, M.; Zelenina, A. S.; Girard, C.; Quidant, R. Parallel and Selective Trapping in a Patterned Plasmonic Landscape. *Nat. Phys.* **2007**, *3*, 477–480.
60. Ling, L.; Guo, H. L.; Zhong, X. L.; Huang, L.; Li, J. F.; Gan, L.; Li, Z. Y. Manipulation of Gold Nanorods with Dual-Optical Tweezers for Surface Plasmon Resonance Control. *Nanotechnology* **2012**, *23*, 215032.
61. Tong, L. M.; Miljković, V. D.; Käll, M. Alignment, Rotation, and Spinning of Single Plasmonic Nanoparticles and Nanowires Using Polarization Dependent Optical Forces. *Nano Lett.* **2010**, *10*, 268–273.
62. Gouesbet, G.; Lock, J. A.; Grehan, G. Generalized Lorenz–Mie Theories and Description of Electromagnetic Arbitrary Shaped Beams: Localized Approximations and Localized Beam Models, a Review. *J. Quant. Spectrosc. Radiat. Transfer* **2011**, *112*, 1–27.
63. Johnson, P. B.; Christy, R. W. Optical Constants of the Noble Metals. *Phys. Rev. B* **1972**, *6*, 4370–4379.